IEEE Access
Multidisciplinary | Rapid Review | Open Access Journal

Received August 6, 2020, accepted August 23, 2020, date of publication September 2, 2020, date of current version September 29, 2020.

Digital Object Identifier 10.1109/ACCESS.2020.3021201

A Broadband High-Gain Circularly Polarized Wide Beam Scanning Leaky-Wave Antenna

YIMING ZHANG[1], HUI LIU[1,2], (Member, IEEE), CHENYANG MENG[1], YUXIN LIN[1], YUAN ZHANG[1], ERIK FORSBERG[2], (Member, IEEE), AND SAILING HE[1,2,3], (Fellow, IEEE)

[1]RF Circuit and Microwave System Laboratory, Centre for Optical and Electromagnetic Research, South China Academy of Advanced Optoelectronics, South China Normal University, Guangzhou 510006, China
[2]RF Circuit and Microwave System Laboratory, Center for Optical and Electromagnetic Research, National Engineering Research Center for Optical Instruments, Zhejiang University, Hangzhou 310058, China
[3]Department of Electromagnetic Engineering, School of Electrical Engineering, KTH Royal Institute of Technology, SE-100 44 Stockholm, Sweden

Corresponding authors: Sailing He (sailing@kth.se) and Hui Liu (liuhuizju@zju.edu.cn)

This work was supported in part by Ningbo Science and Technology (project No. 2018B10093), in part by the National Key Research and Development Program of China under Grant 2018YFC1407500, and in part by the National Natural Science Foundation of China under Grant 61774131 and Grant 11621101.

ABSTRACT A new type of broadband circularly polarized leaky-wave antenna (LWA) with high-gain based on a corrugated substrate integrated waveguide (CSIW) structure is proposed and investigated. The CSIW structure that employs open-circuit stubs to replace metallic vias has the advantages of low-cost and easy fabrication as compared to conventional substrate integrated waveguides. Each unit-cell of the proposed LWA consists of two quarter-wavelength microstrip lines and a half-mode CSIW cell with three open-circuit stubs. Two M-shaped slots etched on the half-mode CSIW cell enables the generation of circularly polarized (CP) radiation. The full LWA, which consists of thirteen matched unit-cells cascaded along the direction of propagation enables continuous backward to forward beam scanning. The properties of the CSIW structure, including impedance matching and phase constant, are analyzed by Bloch impedance and dispersion simulations and the influence of the dimensions of the open-circuit stubs on the CP LWA performance is also investigated. A protype of the proposed LWA is fabricated and characterized. The measured results indicate that the proposed CSIW LWA has a high peak gain (9.3-12.5 dBi) throughout a large beam-scanning angle range from $-28°$ to $+25°$, and the impedance bandwidth and 3-dB axial ratio (AR) bandwidth are over 40% covering the full *Ka*-band.

INDEX TERMS Leaky-wave antenna (LWA), corrugated substrate integrated waveguide (CSIW), circular polarization (CP), beam scanning, *Ka*-band, broadband.

I. INTRODUCTION

Leaky-wave antennas (LWAs) are wave-guiding structures in which a travelling wave radiates through energy leakage along the entirety of the structure [1], [2]. Such antennas have received much attention due to advantages such as high gain, simple feeding network, wide optional bandwidth and unique frequency beam scanning ability [3]–[5]. Using substrate integrated waveguides (SIWs), extensively used for print circuit boards (PCBs) and that have advantageous properties such as low cost, low profile, low loss and easy integration with microstrip and coplanar circuits [6], [7], enables design of LWAs for high frequency bands. However, the metallic vias of SIWs are not suitable for some integrated circuits [8] and, as a solution to this, corrugated SIW (CSIW) structures, which uses open-circuit microstrip stubs in lieu of metallic vias in order to artificially create electric sidewalls, have been proposed [9]. CSIWs maintains DC isolation between the top and bottom conductors through the open-circuit stubs instead of metallic vias. CSIWs thus have the advantages of SIWs while not requiring a cumbersome metallic via fabrication process. An analysis of the dispersion characteristics of the propagating modes of a CSIW structure operating in *X*-band showed that the a CSIW structure with tapered microstrip (even mode) feed can propagate quasi-*TEM* and TE_{10} modes and that a differential (odd mode) feed can excite TE_{10MM} and TE_{20} modes [10]. Thus, CSIW structures operated at frequencies above the TE_{10} mode cutoff are promising candidates

The associate editor coordinating the review of this manuscript and approving it for publication was Raghvendra Kumar Chaudhary.

for LWA design. A high-gain millimeter-wave leaky-wave antenna based on a bent corrugated SIW (BCSIW) with a broad frequency range from 22 to 29.2 GHz and a large beam angle range from −69° to −10° was recently demonstrated [11], and two electronically controlled LWAs that realized beam scanning at fixed frequencies by using loaded varactor diodes [12] and PIN diodes [13] on the CSIW structure have been reported. A circularly polarized (CP) LWA based on a CSIW, which utilized two compound slot pair arrays etched on the top of the antenna to achieve broadside radiation and good axial ration (AR) in the main beam direction, has also been proposed [14].

For long-distance wireless, e.g. satellite, and radar communication systems, an operating frequency in the *Ka*-band (26.5 GHz to 40 GHz) is typically preferred as it enables high data-rate links and miniaturized antenna systems [15]–[17]. When employing LWAs for such systems it is advantageous to utilize CP waves rather than linearly polarized (LP) waves due to the fact that CP LWAs avoids polarization mismatch and also suppresses multipath interference during beam scanning [18]–[20]. Etching various kinds of slots on the surface of an SIW has been widely used to obtain specific polarization characteristics and good impedance matching for LWAs [21]–[28]. A miniaturized frequency-scanning LWA based on a half-mode substrate integrated waveguide (HMSIW) in combination with ramp-shaped slots as interdigital capacitors (IDCs) achieved composite right/left-handed (CRLH) and CP characteristics [24]. In [25] and [26], H-shaped slots etched on the top of SIWs that cut both the transverse and longitudinal currents through the transverse and longitudinal slots, enabled CP wave generation. McMillan *et al.* [28] evaluated the electric fields of microstrip lines and the analyses showed that microstrip transmission lines also allowed a leaky mode. Replacing the SIW delay section of each unit-cell by microstrip lines to reduce the length of periodic LWAs has been previously reported in [21], e.g. the total length of an LWA with five unit-cells was shortened by 24.4% in comparison to an equivalent full waveguide CP LWA [29]. Furthermore, for periodic CP LWAs, the introduction of microstrip lines improves broadside radiation matching as well as CP purity [21], [30]. Compared with [21], a further reduction in size by 33.5% along the scanning plane of the LWA was achieved in [30] by meandering the microstrip line.

In this article we propose a broadband CSIW CP LWA with M-shaped slots based on a CSIW with high gain and wide beam scanning ability. In comparison to our recently reported BCSIW LWA [11], a series-feed microstrip line structure of each unit-cell makes the LWA discussed here more compact in the propagation direction. The M-shaped slots can cut both transverse and longitudinal currents through the slots in different direction in the same fashion as in [25] and [26]. Characterizations of a fabricated prototype of the CSIW CP LWA (referred to as 'LWA' for brevity in the below) confirms a wide impedance bandwidth while maintaining high gain as well as a 3-dB AR bandwidth that is as wide as the impedance bandwidth. The series-feed microstrip line structure furthermore yields high CP purity.

Section 2 of the paper introduces the antenna design and presents an analyzes the design through simulations and section 3 compares experimental characterizations of the fabricated prototype with the simulations and also compares our proposed LWA with previously reported work in section 4. The paper end with a summary in section 5.

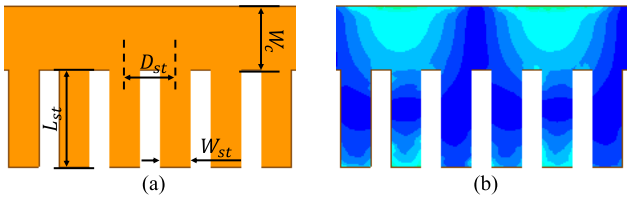

FIGURE 1. (a) Half-mode CSIW (HMCSIW) structure. (b) Electrical field distribution at 31.9 GHz.

II. ANTENNA DESIGN AND ANALYSIS

A. UNIT-CELL DESIGN AND ANALYSIS

We make use of a half-mode CSIW (HMCSIW), the width of which is half that of a full-mode CSIW, as the starting point for the LWA unit-cell design. Fig. 1 shows the HWCSIW structure and simulated electrical field distribution at 31.9 GHz. The HMCSIW supports a field distribution that is close to that of a corresponding SIW as the open edge of HMCSIW is equivalent to the SIW magnetic wall. It can be clearly seen that the proposed HMCSIW support a TE_{10} mode making it possible to design a periodic LWA by employing the same theoretical basis as for design of periodic SIW LWAs.

The unit-cells and top view of the proposed LWA that consists of 13 unit-cells are depicted in Fig. 2 and the

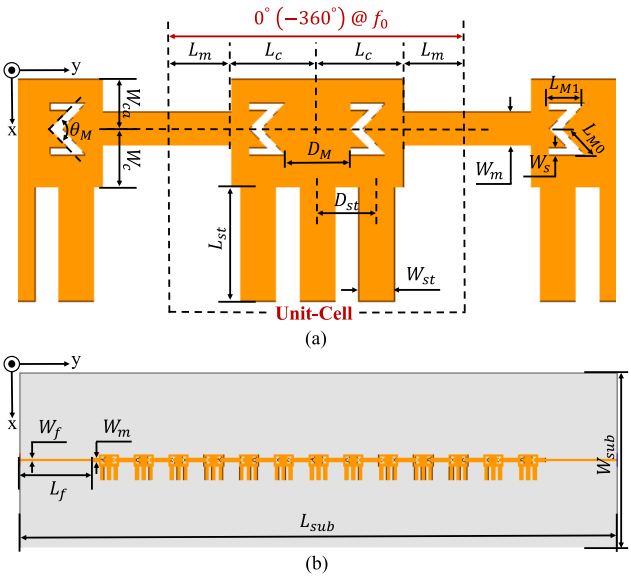

FIGURE 2. Geometry of the proposed LWA: (a) 3 unit-cells (b) top view of the full LWA consisting of 13 unit-cells. The dimensions indicated in the figure are summarized in Table 1.

TABLE 1. Geometry parameters for unit-cell III and the full LWA as depicted in Fig 2.

Parameter	Value	Parameter	Value
L_c	1.6 mm	L_f	11.5 mm
L_m	1.2 mm	L_{st}	2.15 mm
L_{sub}	96.1 mm	L_{M0}	0.65 mm
L_{M1}	0.65 mm	W_c	1.1 mm
W_f	0.42 mm	W_m	0.63 mm
W_s	0.15 mm	W_{ca}	0.95 mm
W_{st}	0.65 mm	W_{sub}	28.0 mm
D_{st}	0.43 mm	D_M	1.23 mm
θ_M	93°		

dimensions are listed in Table 1. The structure is designed on a SYTECH SJ9300 substrate with dielectric constant $\varepsilon_r = 3.0$, loss tangent $\tan\delta = 0.0015$ and height $h = 0.254$ mm. As can be seen in Fig. 2(a), the unit-cell consists of two quarter-wavelength microstrip lines with length L_m and the HMCSIW cell with two M-shaped slots. The full length of one unit-cell is determined to be the wavelength at broadside frequency (f_0). The length of the open-circuit microstrip stubs are initially set as a quarter wavelength of the broadside frequency, however the optimized length is somewhat larger as the unit-cell should give priority to supporting the TE_{10} mode at lower frequencies.

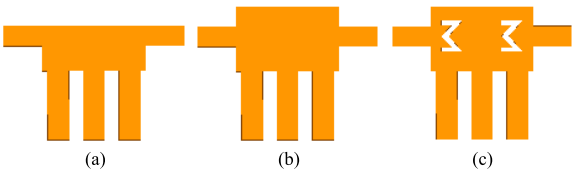

FIGURE 3. Design iteration of the unit-cell; (a) Unit-cell I, (b) Unit-cell II, and (c) Unit-cell III.

The design evolution of the unit-cell is illustrated in Fig. 3; the main structure of the unit-cells consists of two quarter-wavelength microstrip lines and a CSIW cell with three open-circuit microstrip stubs. The first design iteration consists of an HMCSIW cell combined with two microstrip lines. Compared with our previous work [11], the HMCSIW and the two microstrip lines makes for a compact structure, being narrower in width in the x-direction and shorter in length in the y-direction. The straight edge of the HMCSIW acts as the radiator, however the first design iteration cannot generate CP waves. To enable generation of CP waves, slots that can affect the surface currents are needed. The width of the HMCSIW first design iteration is however too narrow to etch slots on it, and for that reason a second iteration unit-cell structure with a wider CSIW cavity (Fig. 3(b), unit-cell II) is introduced, and two M-shape slots are added to this in the final unit-cell iteration structure (Fig. 3(c), unit-cell III).

We analyze the characteristics of the three CSIW unit-cell structures using dispersion and Bloch impedance diagrams. The dispersion diagram can be extracted from the unit-cells'

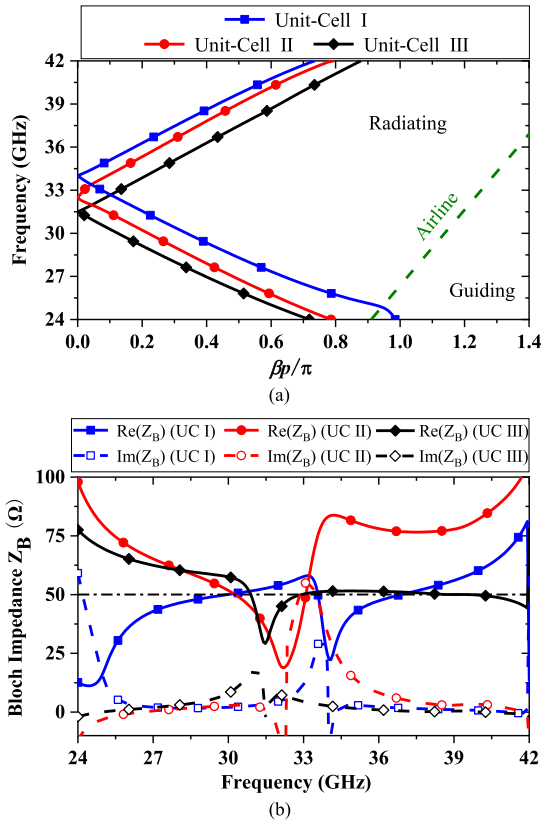

FIGURE 4. Characteristics of the CSIW unit-cell structures. (a) Dispersion diagram. (b) Bloch impedance.

ABCD-parameters or by their S-parameters using

$$\beta p = \text{phase}(A \pm \sqrt{A^2 - 1}) \tag{1}$$

$$\beta p = \cos^{-1}\left[\frac{1 - S_{11}S_{22} + S_{12}S_{21}}{2S_{21}}\right] \tag{2}$$

where β is phase constant and p is the full length of the unit-cell [27], [31]. All S-parameters of the unit-cell can be extracted using fast driven-mode simulation in Ansys HFSS [32]. As shown in Fig. 4(a), the entire frequency range is separated into a guiding range and radiating range as indicated by the plotted airline, the slope of which is $2p\times$ freq/c_0 [27]. The backward and forward radiating regions in the low and high frequency bands respectively are separated by the broadside frequencies (found at the frequency point corresponding to $\beta = 0$ in Fig. 4(a)), and we can observe that the broadside frequency decreases by the widening of the HMCSIW cavity and is further decreased by the introduction of the etched slots. We note that the dispersion curves of all three unit-cell structures have continuous transitions at $\beta = 0$, and we can thus assume that they have no open stopbands (OSBs) in the operating bandwidth and that broadside radiation can be excited at the respective broadside frequency points. We study the impedance matching of the unit-cells using the Bloch impedance diagrams, which can be obtained from the unit-cells' ABCD-parameters or by their

S-parameters using

$$Z_B = \frac{-(A-D) \pm \sqrt{(A+D)^2 - 4}}{2C} \quad (3)$$

$$Z_B = \frac{2jZ_0 S_{21}\sin(\beta p)}{(1-S_{11})(1-S_{22}) - S_{21}S_{12}} \quad (4)$$

where Z_0 is defined as 50 Ω in our design. Real and imaginary parts of the simulated Bloch impedances are shown in Fig. 4(b) for the three unit-cells. For good impedance matching between the unit-cell and the microstrip feed line, the design targets for the real and imaginary parts are 50 Ω and 0 Ω, respectively. It is however difficult to achieve perfect impedance matching at the broadside frequency point and therefore we consider a deviation of 15 Ω in the real part to be good impedance matching. As can be seen in Fig 4(b), although the impedance of unit-cell I is matched in most of the operating bandwidth, there is poor impedance matching at the broadside frequency point (34 GHz) as the real and imaginary parts of unit-cell I at 34 GHz are less than 25 Ω and greater than 30 Ω, respectively. The impedance matching for unit-cell II is worse than that of unit-cell I in the frequency range from 32.5 GHz (the broadside frequency of unit-cell II) to 40 GHz. However, by adding the two etched M-shaped slots in unit-cell III, good impedance matching in achieved throughout the whole *Ka*-band.

In the transmission direction the M-shaped slots can be divided into transverse and longitudinal slots, which cut both transverse and longitudinal currents thereby generating circularly polarized waves in the far field. The circular polarization characteristics can be demonstrated by simulating the unit-cell's axial ratio in the broadside direction (broadside AR). We study the unit-cell's circular polarization characteristics at six equally spaced frequency points in the *Ka*-band. As shown in Fig. 5, the broadside AR is less than 3 dB at all concerned frequency points after the dimensions and intervals of the two M-shaped slots have been optimized. In addition, we simulate the surface current distributions of unit-cell III at 31.9 GHz to further analyze the polarization characteristics and, as can be seen in Fig. 6, the dominant surface current rotates clockwise, which implies that left-handed circularly polarization (LHCP) is achieved [24], [33].

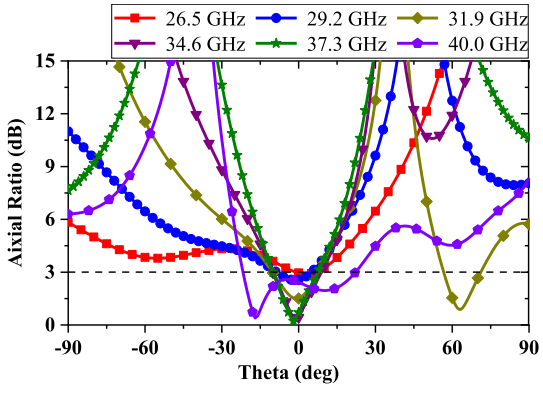

FIGURE 5. Simulated broadside axial-ratio of unit-cell III.

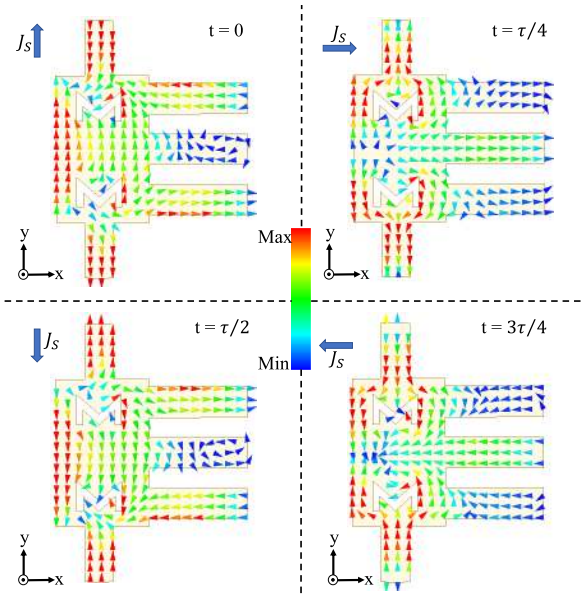

FIGURE 6. Simulated surface current distributions in unit-cell III.

B. SIMULATIONS OF THE FULL LWA

The full LWA consists of thirteen matched unit-cells cascaded along the propagation direction to which two microstrip lines are loaded as the feed line (see Fig. 2(b)). HFSS simulation results of the LWA are shown in Fig. 7. The impedance bandwidth of the S-parameters, plotted in Fig. 7(a), is broad and covers the whole *Ka*-band. The analysis of the simulated surface current distributions indicates that the LWA can radiate a LHCP wave, and, as can be seen in Fig. 7(b), we obtain a peak LHCP gain in the range 10 dB to 13.5 dB in the far-field. Furthermore, the simulated radiation efficiency is greater than 80% in the whole operating bandwidth, with a maximum of 91% at 39 GHz. Beam scanning capability and CP characteristics are studied at six equally spaced frequency points in the *Ka*-band and as can be seen in Fig. 7(c), the proposed LWA has a beam scanning range from −28° to +25°. The axial ratios in the scan plane plotted in Fig 7(d) indicate that CP characteristics is achievable across the whole *Ka*-band.

C. THE EFFECT OF MICROSTRIP STUBS DIMENSIONS ON THE LWA PERFORMANCE

The open-circuit microstrip stubs can be regarded as lumped elements loaded on the side of a microwave device. For certain advanced devices or antennas, special properties can be obtained by using a liquid crystal (LC) substrate or loading varactor diodes on the microstrip stubs. For example, LC-based microwave filters' bandwidth or center frequency can be tuned by changing the LC dielectric constant through a controlling bias [34], and a frequency-fixed beam-scanning LWA [12] was realized by using electronically controllable varactor diodes on corrugated microstrip lines. These examples are all based on the principle of changing the electrical length of the microstrip stubs, which is also equivalent

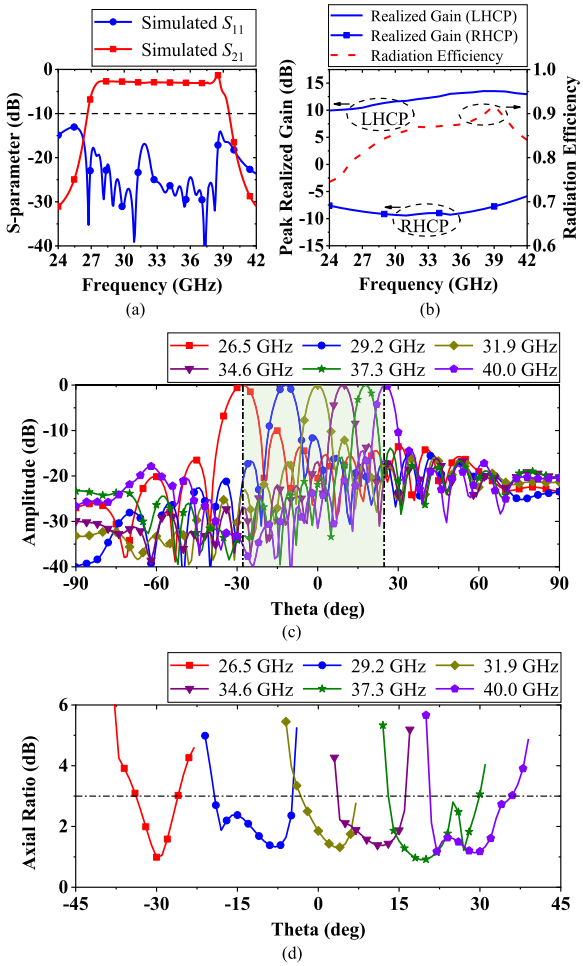

FIGURE 7. Simulated (a) *S*-parameters; (b) antenna gain and radiation efficiency; (c) normalized radiation pattern; and (d) axial ratio for the proposed LWA.

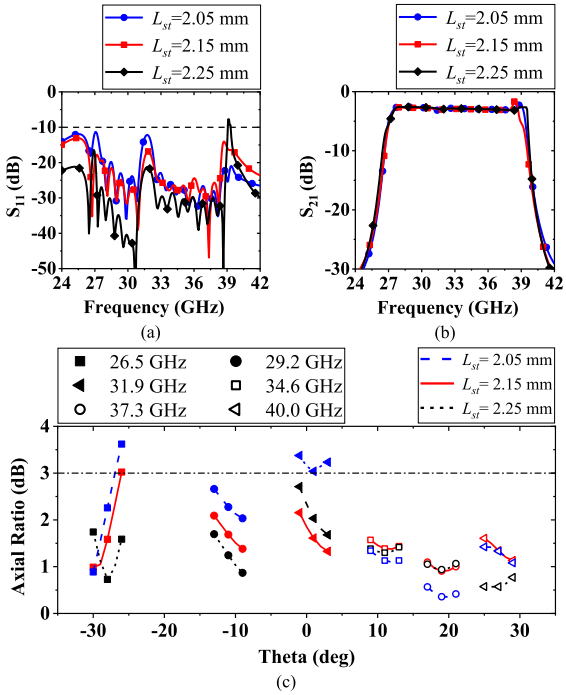

FIGURE 8. Simulated *S*-parameters and AR for the proposed LWA for varying stub lengths, L_{st}.

to minor changes in the physical length or width of the microstrip stubs in a simulation. It is thus worth to study the effect changes of the length and width of the microstrip stubs has on impedance matching and radiating performance of the full LWA.

Keeping all other geometrical parameters of the LWA fixed, we vary the dimensions of the open-circuit microstrip stubs in a small step interval (± 0.1 mm) to study the relationship between the LWA's matching and polarization performances. Given fundamental understanding of CSIWs, it is reasonable to suppose that varying the length of the open-circuit microstrip stubs length would cause offsets of the center frequency of the proposed CSIW LWA. However, as can be seen in Fig. 8, the operating bandwidth does not see any shift in frequency for small changes in the length of the microstrip stubs, which is not consistent with our conjecture, only shifts of S_{11}, especially the open stopband (OSB), are observed. It can be clearly seen that the length of microstrip stubs, L_{st}, has a significant influence on the OSB and the impedance matching at low and high frequencies. An OSB at 31.9 GHz appears when increasing the length of the microstrip stubs. Although S_{11} is less than -20 dB throughout most of the operating bandwidth when $L_{st} = 2.25$ mm, there is a narrow impedance unmatched bandwidth at 39 GHz. S_{21} is not sensitive to the length variation of the microstrip stubs, only a slight change at the high frequency end (at 39 GHz) is observed. Furthermore, we find that the AR is very sensitive to the changes of the stub length when the LWA operates at 31.9 GHz (AR > 3 dB for $L_{st} = 2.05$ mm). Fig. 9 plots *S*-parameters and AR at varying stub widths, W_{st}, and we similarly find that with increasing width of the microstrip stubs an OSB will appear and that the impedance matching is affected at low and high frequencies. On the other hand, S_{21} and AR are not sensitive to changes of the width of microstrip stubs.

From this analysis we can be conclude that avoiding the formation of an OSB is the most important point when designing tunable LWAs by varying the electrical length of the microstrip stubs, e.g. as the appearance of an OSB will degrade LWA far-field characteristics such as AR. Furthermore, for some broadband microwave devices with side-loaded microstrip lines, changing the length and/or width of microstrip lines will not affect the insertion loss, but will affect the impedance matching at the high/low frequencies.

III. MEASURED RESULTS AND DISCUSSIONS

A. EXPERIMENTAL CHARACTERIZATION AND COMPARISON WITH SIMULATIONS

A protype of the LWA with thirteen unit-cells (Fig. 10) was fabricated and experimentally characterized for verification

TABLE 2. Comparison of the LWA proposed in this article with previously published CP LWAs.

Reference	LWA Type	Scan BW (GHz)	3-dB CP BW	Max Gain (dBi)	Scanning Range
[14]	CSIW Compound Slot Pair	16.2 - 16.8 (1.8%)	16.2 - 16.8 (1.8%)	/	$(-90°,-87°)$ 3°
[19]	Modified SIW Transverse Slots	15.5 - 18 (14.9%)	15.9 - 17.2 (7.9%)	12.3	$(+35°,+47°)$ 12°
[22]	SIW Two Paired Slots with $\pm 45°$ Inclined	15.8 - 16.2 (2.5%)	Very limited (<2.5%)	18.9	$(-2°,+2°)$ 4°
[21]	SIW & Microstrip Line Two Interdigital Slots with $\pm 45°$ Inclined	4.2 - 4.85 (14.4%)	4.2 - 4.85 (14.4%)	2.5	$(-25°,+26°)$ 51°
Our work	CSIW & Microstrip Line Edge & Two M-shaped Slots	26.5 - 40 (40.6%)	26.5 - 40 (40.6%)	12.5	$(-28°,+25°)$ 53°

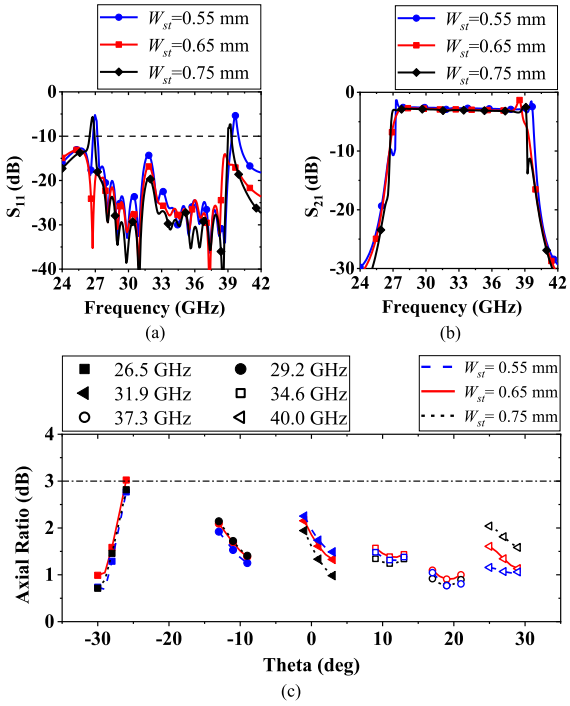

FIGURE 9. Simulated *S*-parameters and AR for the proposed LWA for varying stub widths, W_{st}.

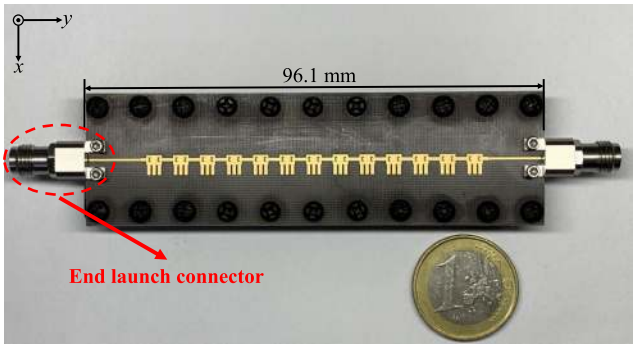

FIGURE 10. Fabricated prototype of the proposed LWA.

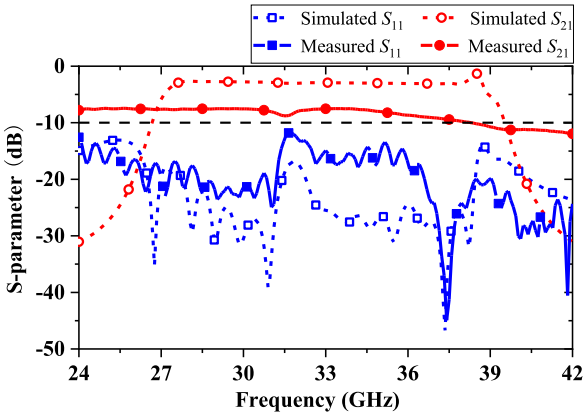

FIGURE 11. Simulated and measured *S*-parameters of the proposed LWA.

of the design. Owing to the softness of the antenna substrate, a plastic clamp is placed at the bottom of the antenna and fixed with acrylic screws to facilitate measurements. An Agilent N5247A network analyzer is used to measure the *S*-parameters of the fabricated LWA, which are plotted together with the simulated *S*-parameters in Fig. 11. The measured S_{21} is somewhat lower than the simulation result, which we attribute to fabrication errors and the unavoidable loss introduced through connector cables as well as the two adaptors (the adaptor insertion loss is $0.05 \times \sqrt{f(\mathrm{GHz})})(\mathrm{dB})$ [11]). The measured impedance bandwidth (defined as the band where S_{11} is below -10 dB) is consistent with the simulation result and covers the full *Ka*-band.

For far-field measurements, one port of the LWA is terminated by a 50 Ω load and the other is used as the feeding port. Fig. 12 plots the simulated and measured far-field results. The measured radiation patterns demonstrate continuous beam scanning from $-28°$ to $+25°$, which is in accordance with the simulation results. The measured realized gain is between 0.5 dB (at 30 GHz) and 1.6 dB (at 36 GHz). The maximum gain of 12.5 dBi is lower than the simulated maximum gain,

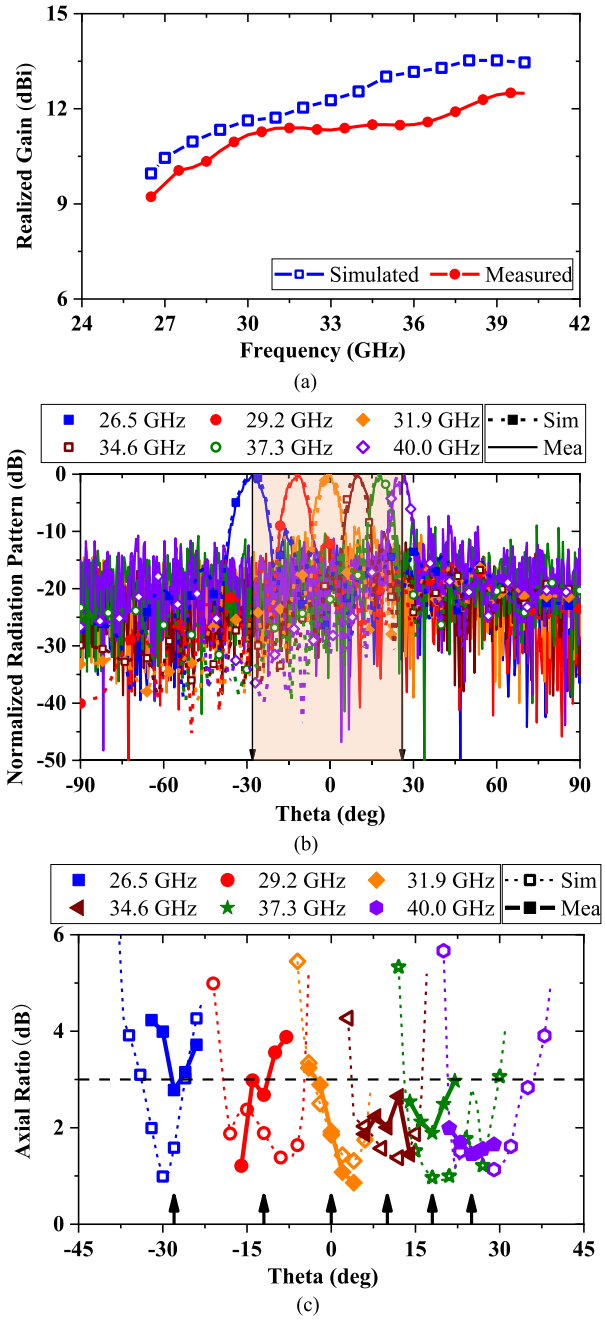

FIGURE 12. Simulated and measured far-field results for the proposed LWA. (a) Realized gain in the *Ka*-band. (b) Normalized radiation patterns in the *yz*-plane at different frequencies. (c) AR in the scan plane at different frequencies.

which also can be attributed to the loss in the adaptors and fabrication errors. The AR is measured in the scan plane for the selected six frequency points and is plotted in Fig. 12(c), and we find the results to be consistent with the simulation result demonstrating that CP can be realized in the whole *Ka*-band. The black arrows in Fig. 12(c) represent the main beam at the corresponding frequency points.

In summary, all measurement results demonstrate that the proposed LWA has a high radiation performance in free space.

B. COMPARISON WITH PREVIOUS WORK

A comparison of pertinent parameters and performance between our proposed CP CSIW LWA and previously published CP LWAs are showed in Table 2. We can see that the impedance bandwidth, the 3-dB CP bandwidth and the scanning range of our proposed LWA are better than those in Refs [14], [19], [21] and [22]. The broad impedance bandwidth is very advantageous for applications that require high scanning resolution. It should furthermore be noted that our proposed LWA can realize continous backward to forward (including broadside) beam scanning without metallic vias and CRLH structures such as interdigital slots.

IV. CONCLUSION

In this article we have presented an improved CSIW LWA with circular polarization characteristics. Compared with our recent work [11], the use of microstrip lines instead of a CSIW delay section gives the proposed CSIW LWA a wider impedance bandwidth. Furthermore, by using a half-mode CSIW structure, the proposed LWA has a more compact size. Two etched M-shaped slots on the CSIW structure enables CP radiation characteristics with frequency scanning. The proposed LWA was analyzed by simulations and a prototype was also fabricated and characterized. The measured impedance bandwidth reached 40.6% covering the whole *Ka*-band (26.5 to 40 GHz) with a peak gain of 12.5 dBi and beam scanning angle ranges from $-28°$ to $+25°$. In addition, the proposed LWA provides an excellent AR bandwidth throughout the *Ka*-band. Hence, the proposed antenna is a very good candidate for millimeter wave applications that requires CP frequency scanning features.

REFERENCES

[1] D. R. Jackson, C. Caloz, and T. Itoh, "Leaky-wave antennas," *Proc. IEEE*, vol. 100, no. 7, pp. 2194–2206, Jul. 2012.

[2] M. K. Mohsen, M. S. M. Isa, A. A. M. Isa, M. K. Abdulhameed, M. L. Attiah, and A. M. Dinar, "Enhancement bandwidth of half width microstrip leaky wave antenna using circular slots," *Prog. Electromagn. Res. C*, vol. 94, p. 5974, 2019.

[3] H. Oraizi, A. Amini, A. Abdolali, and A. M. Karimimehr, "Design of wideband leaky-wave antenna using sinusoidally modulated impedance surface based on the holography theory," *IEEE Antennas Wireless Propag. Lett.*, vol. 17, no. 10, pp. 1807–1811, Oct. 2018.

[4] A. Mahmoodi Malekshah, M. S. Majedi, and A. R. Attari, "Improved design of a SIW long slot leaky wave antenna with low SLL," *IET Microw., Antennas Propag.*, vol. 13, no. 1, pp. 112–117, Jan. 2019.

[5] Y. J. Cheng, W. Hong, K. Wu, and Y. Fan, "Millimeter-wave substrate integrated waveguide long slot leaky-wave antennas and two-dimensional multibeam applications," *IEEE Trans. Antennas Propag.*, vol. 59, no. 1, pp. 40–47, Jan. 2011.

[6] D.-J. Wei, J. Li, J. Liu, G. Yang, and W. Zhang, "Dual-band substrate-integrated waveguide leaky-wave antenna with a simple feeding way," *IEEE Antennas Wireless Propag. Lett.*, vol. 18, no. 4, pp. 591–595, Apr. 2019.

[7] A. Sarkar, S. Mukherjee, A. Sharma, A. Biswas, and M. J. Akhtar, "SIW-based quad-beam leaky-wave antenna with polarization diversity for four-quadrant scanning applications," *IEEE Trans. Antennas Propag.*, vol. 66, no. 8, pp. 3918–3925, Aug. 2018.

[8] D. G. Chen and K. W. Eccleston, "Substrate integrated waveguide with corrugated wall," in *Proc. Asia–Pacific Microw. Conf.*, Dec. 2008, pp. 1–4.

[9] S. Yao, F. Xu, J. Yang, and L. Cao, "Planer slot antenna based on triangle corrugated substrate integrated waveguide cavity," in *Proc. 6th Asia–Pacific Conf. Antennas Propag. (APCAP)*, Xi'an, China, Oct. 2017.

[10] K. W. Eccleston, "Mode analysis of the corrugated substrate integrated waveguide," *IEEE Trans. Microw. Theory Techn.*, vol. 60, no. 10, pp. 3004–3012, Oct. 2012.
[11] Y. Lin, Y. Zhang, H. Liu, Y. Zhang, E. Forsberg, and S. He, "A simple high-gain millimeter-wave leaky-wave slot antenna based on a bent corrugated SIW," *IEEE Access*, vol. 8, pp. 91999–92006, 2020.
[12] K. Chen, Y. H. Zhang, S. Y. He, H. T. Chen, and G. Q. Zhu, "An electronically controlled leaky-wave antenna based on corrugated SIW structure with fixed-frequency beam scanning," *IEEE Antennas Wireless Propag. Lett.*, vol. 18, no. 3, pp. 551–555, Mar. 2019.
[13] T. Lou, X.-X. Yang, H. Qiu, Q. Luo, and S. Gao, "Low-cost electrical beam-scanning leaky-wave antenna based on bent corrugated substrate integrated waveguide," *IEEE Antennas Wireless Propag. Lett.*, vol. 18, no. 2, pp. 353–357, Feb. 2019.
[14] C. Liu, Z. Li, and J. Wang, "A new kind of circularly polarized leaky-wave antenna based on corrugated substrate integrated waveguide," in *Proc. 5th IEEE Int. Symp. Microw., Antenna, Propag. EMC Technol. Wireless Commun. (MAPE)*, Oct. 2013, Art. no. 383387.
[15] Y. Rahmat-Samii, V. Manohar, J. M. Kovitz, R. E. Hodges, G. Freebury, and E. Peral, "Development of highly constrained 1 m ka-band mesh deployable offset reflector antenna for next generation CubeSat radars," *IEEE Trans. Antennas Propag.*, vol. 67, no. 10, pp. 6254–6266, Oct. 2019.
[16] M. M. Tahseen and A. A. Kishk, "Ka-band circularly polarized high efficiency wide band reflect array using cross bow-tie elements," *Prog. Electromagn. Res.*, vol. 153, pp. 1–10, 2015.
[17] S. Mener, R. Gillard, and L. Roy, "A dual-band dual-circular-polarization antenna for ka-band satellite communications," *IEEE Antennas Wireless Propag. Lett.*, vol. 16, pp. 274–277, 2017.
[18] D. Sanchez-Escuderos, M. Ferrando-Bataller, J. I. Herranz, and V. M. Rodrigo-Penarrocha, "Low-loss circularly polarized periodic leaky-wave antenna," *IEEE Antennas Wireless Propag. Lett.*, vol. 15, pp. 614–617, 2016.
[19] C. Jin, M. Mujumdar, and A. Alphones, "Broadband beam scanning circularly-polarised leaky-wave antenna based on modified substrate integrated waveguide," *Electron. Lett.*, vol. 49, no. 5, pp. 316–318, Feb. 2013.
[20] Q. Zhang, Q. Zhang, and Y. Chen, "High-efficiency circularly polarised leaky-wave antenna fed by spoof surface plasmon polaritons," *IET Microw., Antennas Propag.*, vol. 12, no. 10, pp. 1639–1644, Aug. 2018.
[21] H. Lee, J. H. Choi, C.-T.-M. Wu, and T. Itoh, "A compact single radiator CRLH-inspired circularly polarized leaky-wave antenna based on substrate-integrated waveguide," *IEEE Trans. Antennas Propag.*, vol. 63, no. 10, pp. 4566–4572, Oct. 2015.
[22] P. Chen, W. Hong, Z. Kuai, and J. Xu, "A substrate integrated waveguide circular polarized slot radiator and its linear array," *IEEE Antennas Wireless Propag. Lett.*, vol. 8, pp. 120–123, 2009.
[23] M. Alibakhshikenari, B. S. Virdee, C. H. See, R. A. Abd-Alhameed, F. Falcone, and E. Limiti, "High-isolation leaky-wave array antenna based on CRLH-metamaterial implemented on SIW with ±30° frequency beam-scanning capability at millimetre-waves," *Electronics*, vol. 8, no. 6, p. 642, Jun. 2019.
[24] A. Pourghorban Saghati, M. M. Mirsalehi, and M. H. Neshati, "A HMSIW circularly polarized leaky-wave antenna with backward, broadside, and forward radiation," *IEEE Antennas Wireless Propag. Lett.*, vol. 13, pp. 451–454, 2014.
[25] S.-L. Chen, D. K. Karmokar, Z. Li, P.-Y. Qin, R. W. Ziolkowski, and Y. J. Guo, "Circular-polarized Substrate-Integrated-Waveguide leaky-wave antenna with wide-angle and consistent-gain continuous beam scanning," *IEEE Trans. Antennas Propag.*, vol. 67, no. 7, pp. 4418–4428, Jul. 2019.
[26] J. Liu, X. Tang, Y. Li, and Y. Long, "Substrate integrated waveguide leaky-wave antenna with H-Shaped slots," *IEEE Trans. Antennas Propag.*, vol. 60, no. 8, pp. 3962–3967, Aug. 2012.
[27] M. M. Sabahi, A. A. Heidari, and M. Movahhedi, "A compact CRLH circularly polarized leaky-wave antenna based on substrate-integrated waveguide," *IEEE Trans. Antennas Propag.*, vol. 66, no. 9, pp. 4407–4414, Sep. 2018.
[28] L. O. McMillan, N. V. Shuley, and P. W. Davis, "Leaky fields on microstrip," *Prog. Electromagn. Res.*, vol. 17, 1997, Art. no. 323337.
[29] H. Lee, J. H. Choi, Y. Kasahara, and T. Itoh, "A circularly polarized single radiator leaky-wave antenna based on CRLH-inspired substrate integrated waveguide," in *IEEE MTT-S Int. Microw. Symp. Dig.*, Tampa, FL, USA, Jun. 2014, pp. 1–3.
[30] D. Ren, H. Lee, and J. H. Choi, "Bi-directional active and passive meandered circularly polarized CRLH-inspired leaky-wave antennas based on substrate integrated waveguide," in *IEEE MTT-S Int. Microw. Symp. Dig.*, San Francisco, CA, USA, May 2016, pp. 1–4.
[31] A. Sarkar, M. Adhikary, A. Sharma, A. Biswas, M. J. Akhtar, and Z. Hu, "Composite right/left-handed based compact and high gain leaky-wave antenna using complementary spiral resonator on HMSIW for ku band applications," *IET Microw., Antennas Propag.*, vol. 12, no. 8, pp. 1310–1315, Jul. 2018.
[32] *Left-Handed Metamaterial Design Guide*, Ansoft Corp., Pittsburgh, PA, USA, 2007.
[33] J. Li, H. Liu, S. Zhang, M. Luo, Y. Zhang, and S. He, "A wideband single-fed, circularly-polarized patch antenna with enhanced axial ratio bandwidth for UHF RFID reader applications," *IEEE Access*, vol. 6, pp. 55883–55892, 2018.
[34] W. Xu, Y. Zhang, Y. Peng, J. Wang, L. Mu, B. Yu, and H. Zhang, "Tunable bandstop HMSIW filter with flexible center frequency and bandwidth using liquid crystal," *IEEE Access*, vol. 7, pp. 161308–161317, 2019.

YIMING ZHANG was born in Xianyang, China. He received the B.S. degree in electronic science and technology from the Shaanxi University of Science and Technology, Xi'an, China, in 2016. He is currently pursuing the M.S. degree in electromagnetic field and microwave technology with the Centre for Optical and Electromagnetic Research, South China Academy of Advanced Optoelectronics, South China Normal University, Guangzhou, China. His current research interests include microwave components, RF circuits, RFID antennas, mm-wave antennas, and arrays.

HUI LIU (Member, IEEE) was born in Zhumadian, China. He received the M.S. degree in electromagnetic field and microwave technology from South China Normal University, China, in 2013, and the Ph.D. degree in microelectronics and solid state electronics from the Centre for Optical and Electromagnetic Research, South China Academy of Advanced Optoelectronics, South China Normal University, in 2018. He is currently a Postdoctoral Researcher with the Center for Optical and Electromagnetic Research, Zhejiang University. His research interests include antenna, RF circuits, and microwave components.

CHENYANG MENG was born in Kaifeng, China. He received the B.S. degree in communication engineering from Xuchang University, Xuchang, China, in 2013. He is currently pursuing the M.S. degree in electrical engineering with the Centre for Optical and Electromagnetic Research, South China Academy of Advanced Optoelectronics, South China Normal University, Guangzhou, China. His current research interests include leaky-wave antennas and arrays.

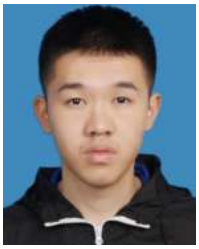

YUXIN LIN was born in Foshan, China. He received the B.S. degree in physics from South China Normal University, China, in 2018, where he is currently pursuing the M.S. degree in electrical engineering. His current research interests include leaky-wave antennas and arrays.

YUAN ZHANG was born in Shanxi, China, in 1980. He received the bachelor's and Ph.D. degrees in optical engineering from the Beijing Institute of Technology, Beijing, China, in 2003 and 2009, respectively. Since 2009, he has been with Nanyang Technological University, Singapore, and Zhejiang University, Zhejiang, China, since 2010, as a Postdoctoral Fellow. Since 2014, he has been a Faculty Member with the Centre for Optical and Electromagnetic Research, South China Normal University, Guangzhou, China. His research interests include metamaterials and artificial electromagnetic structures with interesting properties.

ERIK FORSBERG (Member, IEEE) received the M.Sc. degree in engineering physics and the Ph.D. degree in photonics from the KTH Royal Institute of Technology, Sweden, in 1996 and 2003, respectively. He also studied business and economics at the Stockholm School of Economics, Sweden. Since 2000, he has been a Visiting Scientist with Hokkaido University, Japan, and a Postdoctoral Fellow with the KTH Royal Institute of Technology, in 2003. He was a Faculty Member with Zhejiang University (ZJU), China, between 2004 and 2008. From 2009 to 2012, he was the Founding Graduate Dean (associate) with the Higher Colleges of Technology (HCT), United Arab Emirates. In 2013, he rejoined ZJU as an Associate Professor. His current research interests include nano-lasers, plasmonics, and optical fiber devices.

SAILING HE (Fellow, IEEE) received the Licentiate and Ph.D. degrees in electromagnetic theory from the KTH Royal Institute of Technology, Stockholm, Sweden, in 1991 and 1992, respectively. He has been with the Department of Electromagnetic Engineering as an Assistant Professor, an Associate Professor, and a Full Professor. He is currently a Professor with the Centre for Optical and Electromagnetic Research, Zhejiang University, China. He has first authored one monograph (Oxford University Press) and authored or coauthored over 600 articles in refereed international journals. He has given many invited/plenary talks in international conferences and has served in the leadership for many international conferences. His current research interests include electromagnetic metamaterials, optoelectronics, sensing, and communication.